Published in final edited form as:
Brain Res. 2009 January 16; 1249: 135–147. doi:10.1016/j.brainres.2008.10.058.

Vagal innervation of the aldosterone-sensitive HSD2 neurons in the NTS

Jung-Won Shin, **Joel C. Geerling**, and **Arthur D. Loewy**
Department of Anatomy and Neurobiology, Washington University School of Medicine, St. Louis, MO 63110, USA

Abstract

The nucleus of the solitary tract (NTS) contains a unique subpopulation of aldosterone-sensitive neurons. These neurons express the enzyme 11-β-hydroxysteroid dehydrogenase type 2 (HSD2) and are activated by sodium deprivation. They are located in the caudal NTS, a region which is densely innervated by the vagus nerve, suggesting that they could receive direct viscerosensory input from the periphery. To test this possibility, we injected the highly sensitive axonal tracer biotinylated dextran amine (BDA) into the left nodose ganglion in rats. Using confocal microscopy, we observed a sparse input from the vagus to most HSD2 neurons. Roughly 80% of the ipsilateral HSD2 neurons exhibited at least one close contact with a BDA-labeled vagal bouton, although most of these cells received only a few total contacts. Most of these contacts were axo-dendritic (~80%), while ~20% were axo-somatic. In contrast, the synaptic vesicular transporters VGLUT2 or GAD7 labeled much larger populations of boutons contacting HSD2-labeled dendrites and somata, suggesting that direct input from the vagus may only account for a minority of the information integrated by these neurons. In summary, the aldosterone-sensitive HSD2 neurons in the NTS appear to receive a small amount of direct viscerosensory input from the vagus nerve. The peripheral sites of origin and functional significance of this projection remain unknown. Combined with previously-identified central sources of input to these cells, the present finding indicates that the HSD2 neurons integrate humoral information with input from a variety of neural afferents.

Introduction

The nucleus of the solitary tract (NTS) contains a small subgroup of neurons that are sensitive to aldosterone (Geerling et al., 2006a; Geerling et al., 2006b). Due to their expression of the glucocorticoid-inactivating enzyme HSD2 (11-β-hydroxysteroid dehydrogenase type 2), they are referred to as HSD2 neurons. The HSD2 neurons are activated under low-sodium and high-aldosterone conditions including dietary sodium deprivation, hypovolemia, and chronic mineralocorticoid administration, and then inactivated after salt is ingested. This activity pattern, as revealed by c-Fos expression, is the inverse of most other neurons in their region of the NTS (Geerling et al., 2006a; Geerling and Loewy, 2006c; Geerling and Loewy, 2007b; Geerling and Loewy, 2007a).

Correspondence to: Joel C. Geerling, M.D., Ph.D., Department of Anatomy and Neurobiology – Box 8108, Washington University School of Medicine, 660 S. Euclid Ave., St. Louis, MO 63110 USA, Tel: 314-362-3551, Fax: 314-362-3446, E-mail: geerlinj@msnotes.wustl.edu.
Senior Editor: Alan Sved
Associate Editor: Timothy H. Moran

The axonal projections of the HSD2 neurons have been identified in rats (Geerling and Loewy, 2006b), and some multisynaptic output pathways as well (Geerling and Loewy, 2006a; Shekhtman et al., 2007), but their sources of synaptic input remain largely unexplored. A minor input arrives from neurons in an adjacent circumventricular organ, the area postrema, as well as neurotensin-immunoreactive neurons in a neighboring subregion of the NTS that receive baroafferent input (Sequeira et al., 2006). The HSD2 neurons represent a major target of descending axonal projections from neurons in the medial subdivision of the central nucleus of the amygdala (mCeA, Geerling and Loewy, 2006a). Most of the other brain sites that innervate this region of the NTS (Ross et al., 1981; van der Kooy et al., 1984) remain to be explored for direct connections to the HSD2 neurons.

Before identifying central sources of input, we had originally hypothesized that these cells integrate humoral signals from the circulation with neural afferents from the periphery (Geerling et al., 2006a). The HSD2 neurons are uniquely sensitive to blood borne aldosterone (Geerling et al., 2006a), probably due in part to their location in a subregion of the NTS with an incomplete blood-brain barrier (Gross et al., 1990). Aldosterone and other humoral signals may help to modulate the excitability of HSD2 neurons, but synaptic inputs may play just as important, if not more important a role in sculpting their unique pattern of neuronal activation and inhibition.

Based on their location in the caudal NTS, which is the first-order site of termination for the vagus nerve, the HSD2 neurons could receive a major portion of their synaptic input from the periphery. Many of the neurons in this region of the NTS integrate vagal viscerosensory information with modulatory inputs from sites within the brain, and then send output connections to limbic areas of the forebrain which control ingestive behaviors, emotion, and arousal, as well output to nearby regions of the medulla that regulate gastrointestinal, cardiovascular, and respiratory functions (Loewy, 1990).

The general distribution of vagal afferent fibers in the rat NTS has been described in a number of transganglionic transport studies (Norgren and Smith, 1988; Altschuler et al., 1989; Chan et al., 2000). Vagal axons are distributed to the general region inhabited by HSD2 neurons, but no evidence exists regarding whether these particular cells are directly innervated.

Not all neurons in this region of the NTS receive a substantial amount of their input directly from the vagus nerve. In fact, different subtypes of neurons here vary widely with respect to the degree of input they receive directly from the vagus relative to relayed viscerosensory information via local circuitry within the NTS or afferents from other brain regions. For example, large NTS neurons with long ascending projections to the hypothalamus (primarily the A2 noradrenergic neurons, which neighbor the HSD2 group) receive very little direct input from the vagus, in contrast to smaller, intermingled NTS neurons that project to the ventral medulla and receive substantial input from vagal axons (Bailey et al., 2006; Bailey et al., 2007).

In the neuroanatomic experiments described here, we examined the degree to which vagal afferents directly contact HSD2 neurons. To label vagal afferent fibers in the NTS, we injected a highly sensitive axonal tracer (10 kDa biotinylated dextran amine, BDA) directly into the nodose ganglion, which is the collection of pseudounipolar neurons that supply vagal axons centrally to the NTS and peripherally to visceral structures. The HSD2 neurons were systematically analyzed in three animals to determine the general pattern and numbers of potential synapses between BDA-labeled vagal boutons and HSD2-containing dendrites and somata. The degree of vagal input was compared to a broader pattern of appositions between HSD2 neurons and subsets of glutamatergic and GABAergic boutons, marked by their immunoreactivity for the type 2 vesicular glutamate transporter (VGLUT2) and glutamic acid

decarboxylase (GAD67) respectively. As detailed below, the vagus nerve appears to provide relatively sparse direct input to a majority of HSD2 neurons.

Results

BDA injections into the nodose ganglion resulted in extensive axonal labeling in the NTS with an ipsilateral predominance, as shown in Figure 1. In sections ventral to the HSD2 group, many neurons in the ipsilateral dorsal motor nucleus of the vagus nerve (DMX) were weakly labeled with BDA, but no retrogradely labeled cells were found in the sections used for the present analysis. Labeled vagal axons traveling in the solitary tract delimited the medial subdivision of the NTS, in which varying densities of axon terminal labeling were found, including the subregions containing HSD2 neurons.

Roughly 150 HSD2 neurons were analyzed per case (range 141-170, n=3) ipsilateral to the BDA-injected left nodose ganglion. In total, 454 HSD2 neurons and their dendritic arbors were analyzed. In each case, the majority of HSD2 neurons (81 ± 8%, range 73-89%) received at least one close contact from a BDA-labeled bouton. A total of 2196 BDA-HSD2 contacts were counted across all three cases. Of these contacts, 1735 were axo-dendritic (79%) and 461 (21%) were axo-somatic.

Among the roughly 80% of HSD2 neurons that received one or more close contacts from BDA-labeled boutons, 91% (73 ± 8% of the total population) received at least one axo-dendritic apposition, while only 54% (43 ± 7% of the total population) received an axo-somatic contact. Examples of HSD2 neurons receiving multiple axo-dendritic and axo-somatic close contacts are shown in Figure 2.

The number of BDA-labeled boutons contacting any individual HSD2 neuron varied widely. As shown in Figure 3, the overwhelming majority of HSD2 neurons received only a small number of potential vagal synapses, while a select few cells exhibited as many as 28 axo-dendritic contacts. Among HSD2 neurons that received any vagal appositions, the average numbers of axo-dendritic and axo-somatic contacts per cell were 5.2 ± 1.2 and 2.3 ± 0.4, respectively.

The vagal innervation of HSD2 neurons was significantly less dense at the rostral extent of this cell group (adjacent to the fourth ventricle) relative to neurons at or caudal to the obex. This difference is notable in Figure 1 as a low density of BDA axonal labeling in the NTS territory abutting the caudal fourth ventricle, which contains the rostral cluster of HSD2 neurons. When divided arbitrarily by a line extending mediolaterally through the caudal edge of the area postrema (Figure 4), significantly more caudal HSD2 neurons received one or more contacts (89 ± 4%) relative to those in the rostral one-third of this group (62 ± 3%, $p = 0.006$ by two-tailed t-test). Per innervated cell, caudal HSD2 neurons also tended to exhibit more total contacts per cell (6.7 ± 1.4 versus 3.8 ± 1.1 in the rostral cluster), although this difference did not reach statistical significance ($p=0.06$). The numbers of dendritic or somatic contacts per innervated HSD2 neuron did not show statistically significant differences ($p=0.07$ and $p=0.57$, respectively).

These numbers of potential vagal inputs to HSD2 neurons in the NTS were unexpectedly low, so for comparison we performed a similar quantitative assessment of more general markers for synaptic boutons contacting these neurons in a series of n=3 additional rats. As shown in Figure 5, many boutons apposed to HSD2 neurons were labeled with either VGLUT2, which is one of the two major glutamate transporters necessary for fast excitatory neurotransmission in the brain and which is found in many vagal afferents (Corbett et al., 2005;Lachamp et al., 2006;Moechars et al., 2006), or with GAD67, which is one of two GABA-synthesizing enzymes and is necessary for most fast inhibitory neurotransmission in the brain (Asada et al.,

1997). Somatic labeling was not observed for either VGLUT2 or GAD67. These markers produced punctate labeling in mutually exclusive populations of boutons; in our sample of 2059 labeled boutons, none contained both proteins.

The general distribution of HSD2 neurons exhibiting various numbers of contacts from these subtypes of excitatory and inhibitory boutons is shown as a histogram in Figure 6A. The n=30 cells sampled in these three cases received on average a total of 49 ± 4 close contacts from VGLUT2-labeled boutons (range 18-105) and 19 ± 2 from GAD67-labeled boutons (range 6-69). The cellular distribution of VGLUT2 contacts along the surface of an average HSD2 neuron was 26% somatic (range 14 – 55%) versus 74% dendritic (range 45 – 86%). The average cellular distribution of GAD67 contacts was 33% somatic (range 13 – 54%) vs. 67% dendritic (41 – 87%). Relative to VGLUT2-labeled contacts, the percentages of GAD67 axo-somatic and axo-dendritic contacts were significantly different (larger and smaller, respectively; each $p=0.04$), and GAD67 boutons appeared to be located more frequently on thicker, proximal dendrites relative to the more even distribution of VGLUT2-labeled contacts along the entire dendritic arbor. As shown by the histogram in Figure 6B, most HSD2 neurons appear to be contacted by far more VGLUT2-labeled boutons relative to the presumptive vagal inputs identified in the BDA cases described above.

Discussion

These results provide foundational information regarding vagal input to the group of sodium deprivation-activated, aldosterone-sensitive HSD2 neurons in the NTS. BDA-labeled boutons contacting HSD2-labeled cells bodies and dendrites represent potential synaptic input from the vagus nerve. Unexpectedly, in contrast to the generally strong vagal innervation of this region of the NTS, the majority of HSD2 neurons only received a few labeled contacts. With respect to these potential vagal inputs, HSD2 neurons fell into one of four general categories, as summarized in Figure 7: having no close contacts (~20%), axo-dendritic contact only (~40%), axo-somatic contact only (~10%), or contacts on both the soma and one or more dendrites (~30%).

The specific sources of vagal input to the HSD2 neurons, among the wide variety of peripheral structures innervated by branches of the vagus nerve, remain to be identified. Future experiments are necessary to determine the functional significance of this direct innervation, relative to indirect vagal information that is pre-processed by local circuit neurons in the NTS, and relative to other neural afferents and humoral information that is integrated by HSD2 neurons.

Technical considerations

The most important consideration when interpreting the present data is whether they reasonably approximate the degree to which the vagus nerve provides direct synaptic input to HSD2 neurons. Injecting BDA in the nodose ganglion is the most sensitive method available for this type of measurement, producing the most complete and most consistent labeling of vagal afferents to the NTS among various other approaches we have used, including CTb or CTb-HRP injection into the cervical vagus nerve as well as the application of these tracers to the central end of cut nerves (unpublished observations). CTb labels primarily myelinated axons (Robertson and Grant, 1985; LaMotte et al., 1991), which comprise fewer than 20% of fibers in the vagus nerve (Mei et al., 1980).

BDA, on the other hand, indiscriminately labels myelinated and unmyelinated axons in proportion to their numbers within the vagus nerve (Aicher et al., 1999). Applying this tracer directly to vagal afferent cells in the nodose ganglion produces a consistent and uniformly

elevated degree of labeling in comparison with the more variable results after transganglionic transport of other tracers such as CTb applied to the cervical vagus nerve or its distal branches.

It is possible that incomplete anterograde transport of BDA from the nodose ganglion to the NTS results in incomplete filling of some vagal axons in the NTS. As a result, some boutons may have remained unlabeled and therefore not counted. We are not aware of any electron microscopic data revealing the exact proportion of vagal axons that transport BDA centrally after a typical nodose-filling injection, but whether or not it labels fully 100% of the vagal boutons in the NTS, to our knowledge this tracing technique represents the most sensitive methodology currently available for this type of investigation. Some vagal axons exhibited somewhat discontinuous and less-intense labeling, and an occasional bouton-like structure was not included for analysis when no continuity could be established with a parent axon. The vast majority of bouton-like labeling in our images was, however, unambiguously linked to a parent axon, so this particular concern represents at most a minor source of error.

Quantitative aspects of vagal input to the HSD2 neurons

Beyond the tracer methodology used here, additional factors merit consideration with respect to whether the present findings either underestimate or overestimate the true numbers of vagal synapses on HSD2 neurons. The present anatomic findings suggest that direct vagal innervation of HSD2 neurons is rather sparse, but certain considerations suggest that the present results could underestimate the actual number of HSD2 neurons innervated by the vagus, or the numbers of vagal synapses per innervated HSD2 neuron. For example, the right vagus nerve could carry a different amount or type of afferent fibers to HSD2 neurons than the left, which was examined here. Likewise, contralateral projections (not quantified here) may contribute a larger total number of inputs to the ipsilateral HSD2 neuron population, although even if the number of contacts per neuron were doubled, direct vagal innervation would still represent a small fraction of the excitatory input to most HSD2 neurons compared with the number of VGLUT2-labeled contacts.

Additionally, some inputs to their distal dendritic branches or dendritic spines may have gone unnoticed if these parts were not labeled by HSD2 immunofluorescence. To identify these neurons and their dendrites, we relied upon immunolabeling for HSD2 protein, the abundance of which was maximized here by chronic dietary sodium deprivation. This enzyme is found within the endoplasmic reticulum (Odermatt et al., 1999), which extends throughout dendritic arbors and even into axons (Martone et al., 1993; Cooney et al., 2002). Dendritic processes labeled with HSD2 were followed without difficulty over long distances, ranging from as little as 200 μm to over 600 μm from the cell body. Most dendrites fell near the middle of these limits – well within the range of measurements taken from NTS neurons individually filled with biocytin (Okada et al., 2006). Exploring the possibility of vagal projections to hypothetical parts of dendrites that do not contain detectable HSD2 protein would require a better marker for these neurons, or the introduction of a transgene that better fills their dendritic arbors.

Finally, these data may have underestimated the degree of axo-dendritic input to the HSD2 neurons due to the fact that we only analyzed the dendrites of HSD2-ir cell bodies located within the tissue section. This potential confound was mitigated by using thick (200 μm) tissue sections cut in the dominant plane of orientation for most of the dendrites of HSD2 neurons. Accordingly, the majority of HSD2-labeled dendrites either terminated within the image stack containing the parent cell body or could be followed through contiguous image stacks, and clearly terminated before exiting the tissue section.

On the contrary, other considerations suggest that the present results overestimate the degree of direct vagal input to the HSD2 neurons. Unlike the examples of a densely-contacted neuron and dendrite shown in Figure 2, the typical HSD2 neuron displayed between zero and a handful

of total contacts across its entire dendritic arbor, far below the density of inputs from the central nucleus of the amygdala that were identified via a less efficient labeling technique (see Figure 2 of Geerling and Loewy, 2006a). Many or most of the vagal appositions identified here probably represent synaptic contacts (the determination of which will require electron microscopic analysis), but an unknown number may instead synapse upon an adjacent structure in the neuropil, yet lie adjacent to an HSD2-labaled structure simply by chance. The precision of our criteria for determining a "contact" by confocal microscopy is only ~0.5 μm (much greater than the width of a synapse), and depends in part upon empirically-determined laser and detector settings on the instrument. Inherent even to optimal confocal settings is the fact that boutons more densely filled with BDA exhibit correspondingly more intense fluorescence and, even in an ideal confocal image, may sometimes fluoresce into an additional pixel or two beyond the space occupied by tracer labeling within the tissue. The same confound potentially exists for any hotspots of HSD2 protein labeling near a cell membrane, and could lead to the inclusion of certain pairs of structures as "close contacts" which are not directly apposed in the tissue.

In any case, the present findings clearly demonstrate that the vagus nerve itself is probably not a major source of direct synaptic input to the HSD2 neurons. Estimates regarding the total number of synapses per neuron vary widely across different regions of the brain, from ~500-700 for granule cells in the cerebellum to ~1,000-2,000 for neurons in the superior colliculus and as many as 10,000-20,000 for pyramidal cells in the cerebral cortex (Bedi et al., 1980; Mackay and Bedi, 1987). It is not known exactly how many synapses are integrated by neurons in the NTS, most of which are smaller with less extensive patterns of dendritic arborization. Nonetheless, it does not seem unreasonable to speculate that the total number of synapses per large NTS neuron with extra-nuclear projections, such as those in the HSD2 group, is at least in the hundreds. This point is underscored by the numbers of VGLUT2- and GAD67-labeled contacts per HSD2 neuron identified here (20-105 and 6-69, respectively) using the same counting criteria as for BDA-labeled vagal contacts. These numbers are lower bounds on the total number of potential synaptic inputs to HSD2 neurons because VGLUT2 and GAD67 only label subtypes of glutamatergic or GABAergic boutons and do not label some monoaminergic terminals.

By comparison, the presence of just a few BDA-labeled contacts on most HSD2 neurons suggests that the vagus nerve itself provides only a small fraction of their synaptic input. Thus, if the activation of HSD2 neurons is strongly influenced by viscerosensory information carried by the vagus nerve, they are most likely affected via second- or higher-order intranuclear projections, following integration and pre-processing by lower-level local microcircuitry within the NTS.

Possible peripheral sources of vagal afferents to the HSD2 neurons

The peripheral branches of the vagus nerve provide afferent information to the NTS from many different visceral structures, beginning with chemoreceptors in the airway and upper digestive tract (larynx and pharynx), through structures in the thorax (esophagus, tracheo-bronchial system and lungs, aortic baroreceptors, cardiopulmonary volume-sensitive afferents) and, most prominently, gastrointestinal organs in the abdomen. The present data provide no information regarding any of the end-organ source(s) or functional subtypes of vagal afferent fibers which supply information to HSD2 neurons. Certain vagally-innervated viscera, however, are more likely than others based on a comparison between the distribution of HSD2 neurons (Geerling et al., 2006b) and the subnuclear patterns of vagal terminals labeled from various target organs or nerve branches in previous transganglionic tracing studies.

Vagal and glossopharnygeal afferents from in the larynx, pharynx, and soft palate terminate rostral and lateral to the HSD2 neurons, in the intermediate NTS near the solitary tract

(Altschuler et al., 1989). Esophageal afferents selectively innervate the central subnucleus of the NTS (Altschuler et al., 1989), which is distant laterally from the rostral cluster of HSD2 neurons. Most NTS neurons that receive respiratory afferents are located far from the HSD2 neurons in or near the lateral NTS and in the caudal commissural region (Kubin et al., 2006). A minor component of baroafferent input from the aortic depressor nerve (Chan et al., 2000) may overlap a small portion of the HSD2 neuronal distribution, although the majority of baroafferent fibers and terminals target subregions of the NTS dorsal and lateral to them and most of their dendrites. Ganglionic cell bodies of the glossopharnygeal (IX) nerve lie in close proximity to those in the nodose ganglion (Altschuler et al., 1989), allowing that afferents in this nerve, which transmit chemosensory and baroreceptor information from the carotid body and carotid sinus, may have been labeled using our technique and may have contributed a small portion of the BDA-labeled axons in the caudal NTS. Arguing against the likelihood of direct baroafferent input, no HSD2 neurons are among the prominent subsets of NTS neurons that exhibit c-Fos activation following sustained baroafferent (phenylephrine-induced hypertension), nor are they among the larger contingent of neurons in the medial NTS that exhibit c-Fos activation after hydralazine-induced hypotension (unpublished observations, JCG, ADL, and P. Guyenet).

The overwhelming majority of vagal input to the region of the caudal NTS that contains HSD2 neurons is provided by subdiaphragmatic branches to abdominal viscera (Norgren and Smith, 1988). The majority of afferents from the abdomen transmit information from the stomach, which supplies numerous mechanosensitive and possibly chemosensitive fibers to many subnuclei within the medial subdivision of the caudal NTS. Other abdominal organs providing afferents to this region of the NTS may include lesser inputs from the small intestine, pancreas, cecum and possibly the entire colon in rat (Altschuler et al., 1991; Altschuler et al., 1993), and possibly components within the liver and/or portal venous system (Rogers and Hermann, 1983; Norgren and Smith, 1988; Berthoud et al., 1992). Among these structures, the liver and portal venous system could be of interest with respect to the afferent control of HSD2 neurons due to evidence suggesting a vagal sensory mechanism that aids in the early detection of altered osmotic or sodium balance immediately after food and fluids are absorbed from the gut, which allows anticipatory adjustments in behavior and autonomic function that prevent large back-and-forth swings in extracellular osmolarity.

Potential role of vagal afferents in the functional activation and/or inactivation of HSD2 neurons

The basic pattern of HSD2 neuron functional activation, as presently understood from c-Fos studies, is as follows. First, HSD2 neurons are activated progressively by chronic dietary sodium deprivation (with or without overt volume depletion; Geerling et al., 2006a; Geerling and Loewy, 2007b; Geerling and Loewy, 2007a). Second, HSD2 neurons are rapidly inactivated after salt ingestion (Geerling et al., 2006a; Geerling and Loewy, 2006c; Geerling and Loewy, 2007b).

Initially, we hypothesized that the activation of HSD2 neurons during sodium deprivation was due to the progressive increase in circulating aldosterone, acting in concert with unidentified afferents in the vagus nerve (Geerling et al., 2006a). This still could be the case, but the present results seem more consistent with the possibility that the vagus nerve itself exerts only a weak direct influence. Accordingly, direct stimulation of either of the subdiaphragmatic vagus nerves, which provide the vast majority of viscerosensory input to the HSD2 subregion of the NTS, produces a mild and inconsistent increase in c-Fos labeling in a minority of HSD2 neurons, despite a marked elevation in c-Fos labeling across much of the ipsilateral medial NTS (unpublished observations, JCG, ADL, and H. Morita). If this nerve does play a physiologically significant role in activating HSD2 neurons during sodium deprivation, it is

unclear what type(s) of signal it conveys, or from which part(s) of the body this information arises. Some investigators have found evidence for a small complement of hypoosmolar or low-sodium-sensitive afferent fibers in subdiaphragmatic vagal branches that may innervate the portal venous system (Kahrilas and Rogers, 1984), although others have found evidence primarily for hyperosmolar or high-sodium chemosensitive afferents (Andrews and Orbach, 1975; Morita et al., 1997).

Contrary to our original hypothesis that vagal input activates the HSD2 neurons, physiologic evidence suggests that signals delivered to the NTS by the vagus may instead cause their *in*activation. Rats with highly active HSD2 neurons (due to dietary sodium deprivation or chronic mineralocorticoid administration) avidly ingest large amounts of hypertonic saline. Less than 1-2 hours after they begin drinking 3% NaCl, a large population of neurons in the medial NTS exhibits marked c-Fos activation, whereas labeling in the HSD2 neurons decreases back to control levels (Geerling et al., 2006a; Geerling and Loewy, 2006c; Geerling and Loewy, 2007b). Administering hypertonic saline by intra-abdominal injection produces a similar pattern of c-Fos activation in the medial NTS, and likewise suppresses even the low baseline level of c-Fos labeling in HSD2 neurons (see Fig. 1C of Geerling and Loewy, 2007a).

The inhibition of HSD2 neurons by salt ingestion occurs even when the initial stimulus for their activation (and for sodium appetite) is mineralocorticoid administration, which does not produce a physiologic sodium deficit. This finding suggests that their inactivation does not result simply from the loss of excitatory stimuli related to sodium deficiency, but is instead produced by an active inhibitory mechanism stimulated following the ingestion of salt (Geerling and Loewy, 2006c). Sodium hypertonicity may drive this inhibition by stimulating afferents from the abdomen that transmit some combination of information related to mechanical distention and hyperosmolarity (and/or hypernatremia) in the gut and portal venous system. Such vagal viscerosensory afferents would excite their direct target neurons in the medial subdivision of the NTS (virtually all vagal fibers here release the excitatory transmitter glutamate; Smith et al., 1998), which may secondarily inhibit HSD2 neurons via local circuit connections. Alternative possibilities, not exclusive of a vagal mechanism, include the inhibition of HSD2 neurons by osmosensory or sodium-sensory neurons in the area postrema (Sequeira et al., 2006) or via descending projections from the paraventricular nucleus of the hypothalamus or the central nucleus of the amygdala. In any case, the inhibition of HSD2 neurons is likely mediated through the excitation of local GABAergic interneurons within the NTS, except in the case of the CeA, whose GABAergic neurons directly innervate HSD2 neurons (Geerling and Loewy, 2006a). Direct electrophysiologic investigation of local NTS microcircuitry will be necessary to explore these possibilities.

Conclusions

Most of the aldosterone-sensitive, sodium appetite-activated HSD2 neurons in the NTS appear to receive sparse input from the vagus nerve. The source(s) and modalities of information transmitted to them by the vagus remain undiscovered, and the relative functional weight of direct vagal innervation in comparison to their other, more numerous synaptic inputs remains unknown. Given the anatomical evidence for central afferents to HSD2 neurons, as well as functional-anatomical data revealing their unique patterns of activation and inactivation, any major influence of the vagus over these neurons is probably mediated multisynaptically, through local microcircuitry within the NTS, and may thereby play a greater role in driving their inactivation after salt ingestion, rather than their excitation during chronic sodium deprivation.

Experimental procedure

Experimental protocols were approved by the Washington University School of Medicine Institutional Animal Care and Use Committee and conformed to NIH guidelines.

Male Sprague-Dawley rats weighing 220-270g (n=10; Harlan, Indianapolis, IN) underwent dietary sodium deprivation, a treatment that increases the intensity of immunofluorescence labeling for HSD2 within the specialized group of aldosterone-sensitive neurons in the NTS. This increase in HSD2-immunoreactivity, which presumably reflects an increase in protein expression driven by elevated levels of aldosterone (Geerling et al., 2005; Geerling and Loewy, 2006c; Geerling and Loewy, 2007b), allows a complete and consistent visualization of the neurons and their dendritic arbors. As in our previous experiments, rats were housed individually during sodium deprivation with daily cage changes to prevent any re-ingestion of excreted sodium. They were kept on a 12h/12h automated light/dark cycle and provided *ad libitum* access at all times to distilled water (dH2O) and an extremely low sodium chow (<0.01% Na, #85292, Herlan-Teklad, Madison, WI, USA).

BDA anterograde injections

After 7-9 days of dietary sodium deprivation as described above, each rat was anesthetized with sodium pentobarbital (35 mg/kg i.p.). The left cervical vagus nerve was isolated from surrounding tissues and exposed up to the nodose ganglion. A glass micropipette (tip diameter 25 μm) containing the anterograde tracer BDA (10% solution of 10kD BDA in 0.1 M potassium phosphate-buffered saline; Molecular Probes, Eugene, OR) was inserted under the sheath of the nerve peripheral to the nodose ganglion and advanced into it as described previously by Aicher and colleagues (2000). The ganglion was filled by pressure-injection in two to four separate advances through the nerve (total volume ~2μl). Diffusion throughout the nodose ganglion and lack of extra-ganglionic spillage was verified by direct visualization of a small amount of Fast Green dye added to the BDA solution (#F-7252; Sigma, Saint Louis, MO). After the injections, the area was rinsed thoroughly with saline.

After BDA injection, dietary sodium deprivation was continued for an additional 7 days to allow maximal anterograde transport of BDA from labeled neurons in the nodose ganglion throughout their axon terminals in the NTS. Then, rats were anesthetized with sodium pentobarbital (50mg/kg i.p.), and perfused through the aorta with isotonic saline followed by 4% paraformaldehyde in 0.1M sodium phosphate buffer (pH=7.4). Rats used for VGLUT2 +GAD67+HSD2 triple-immunofluorescence (n=3 male Sprague-Dawley 236-373g) were sodium deprived for 9d without BDA injection, and perfused similarly.

Histology

After overnight fixation in 4% paraformaldehyde, 200 μm thick sections were cut through the dorsal one-half of the caudal medulla in the horizontal plane using a freezing microtome. Sections were then permeabilized and blocked for up to 4h in 1% Triton X-100 (Sigma) in 0.01 M potassium phosphate-buffered saline (KPBS) containing 5% donkey serum (Jackson Immunochemicals, West Grove, PA), and then washed twice in KPBS.

Sections from BDA-injected cases were incubated with an affinity-purified sheep polyclonal antibody raised against rat HSD2 (1:40,000; product #1296; Chemicon International, Temecula, CA) in 5% donkey serum for 40-48h at room temperature on a shaker. After two 10 min washes in KPBS, sections were transferred for 5h into a mixture of Cy2-conjugated donkey anti-sheep (1:500, Jackson) and Cy-3 conjugated streptavidin (to label BDA; 1:500, Jackson).

Sections from non-injected cases (n=3) were incubated in a mixture of three primary antibodies: the same sheep anti-HSD2 (1:40,000), a guinea pig polyclonal antiserum specific for rat VGLUT2 (1:25,000; #AB5907, Chemicon), a mouse monoclonal anti-GAD67 antibody (1:500; #MAB5406, Chemicon). After two 10 min washes in KPBS, sections were transferred into a mixture of three fluorophore-conjugated donkey secondary antisera specific for each of the three primary antibody species (Cy5-donkey anti-sheep, Cy3-donkey anti-guinea pig, and Cy2-donkey anti-mouse, all 1:500; Jackson).

After two final washes in KPBS, all sections were mounted on gelatin-coated glass slides and allowed to dry for >1h. Glass coverslips were applied atop a fade-retardant solution of *n*-propyl gallate and sodium azide in glycerol, and then secured around the edges using fingernail polish before confocal imaging with oil objectives.

Case selection and confocal imaging

Our objective was to obtain high-quality cases for unimpaired analysis of the general relationship between vagal afferents and HSD2 neurons. Criteria for inclusion were (1) complete intra-operative filling of the nodose ganglion without extra-ganglionic spillage by visualization of intermixed Fast Green, (2) maximum filling of vagal axons and terminals throughout the NTS, (3) maximum immunoreactive labeling of the HSD2 neurons and their dendrites, (4) a horizontal sectioning angle that captures the maximum amount of the HSD2 population throughout its rostro-caudal extend in one central 200 μm-thick section, and (5) the ability to image the entire area of interest (the HSD2 neuron-containing subregion of the NTS) without interference from histological artifacts such as torn tissue, overlying debris, or cross-reactive material remaining in overlying blood vessels. Three such cases were obtained for analysis (case #2187, 2188, and 2193).

All confocal imaging was performed using an Olympus Fluoview FV500b laser-scanning microscope. The large montage images shown in Fig. 1 were acquired as multiple individual stacks using a 20x oil objective (NA 1.17) in 1 μm z-steps throughout the full tissue depth. For these displays, 90-120 z-frames from were collapsed into a single two-dimensional, maximum-projection image to produce individual tiles (642 × 642 μm) each at a resolution of 1024 × 1024 pixels (thus the minimum unit of resolution, one pixel, covers roughly 0.6 × 0.6 μm). Individual 2D panels were then aligned into large-area photomontages using Adobe Photoshop.

The images shown in Figs. 2 and 5 were taken with a 60x oil objective (NA 1.4) in 0.5 μm z-steps. These images, compiled of 20-25 z-frames (Fig. 2, depth of 10-12 μm through the z-axis) and 17 z-frames (Fig. 5, depth of 8.5 μm through the z-axis), were extracted from a thicker stack of confocal planes to show examples of close contacts with a specific HSD2 neuron. All appositions shown in these images were verified by examining the individual optical planes.

Manipulation of confocal stacks and z-frame compression was performed with MetaMorph software (Molecular Devices, Sunnyvale, CA, USA). Pseudocoloration of these images and uniform brightness and contrast adjustments were performed in Photoshop. 3D reconstructions were performed on selected stacks using in MetaMorph software.

Data analysis

In all cases, the data from individual 20x confocal stacks encompassing the entire ipsilateral population of HSD2 neurons, such as those shown in Figure 1, were used to search HSD2 neurons for close contacts from the vagus nerve (BDA-injected cases) or from VGLUT2- and GAD67-immunoreactive boutons. Here, the terms “close contact” and also “apposition” are used to indicate a labeled bouton (generally 2-6 pixels in diameter, or 1-3 μm) immediately adjacent to an HSD2-labeled soma or dendrite in any three-dimensional direction (either

apposed within the X-Y plane of one or more single optical planes or at the same X-Y location in one or more planes directly atop or beneath an HSD2-labeled structure, i.e. immediately in front of or behind it) with no unlabeled pixels between the two structures for at least one pixel-width of contact. Determining whether any or all points of contact between a bouton and an HSD2 neuron form actual synapses requires electron microscopic analysis and is therefore is not within the purview of the present dataset. These appositions, or close contacts, simply represent potential sites at which synapses upon HSD2 neurons may exist.

Inherent to confocal imaging of labeled animal tissue is a signal-to-noise problem in which scattered individual background pixels may obfuscate analysis. To guard against this possible confound, BDA-labeled boutons (*en passant* or terminal) were only counted if they appeared to be continuous with a BDA-labeled axon. Occasional pixels exhibiting no apparent continuity with a BDA-filled axon were assumed to represent background noise. Most boutons were clearly discernable as *en passant* and terminal swellings and were obviously continuous with and easily distinguishable from their parent axons.

From each case, one horizontal section containing the most HSD2 neurons was chosen for analysis. This section was the most prominent central section out of a total of 3-4 contiguous horizontal sections per case that together contain the entire population of HSD2-immunoreactive neurons in the NTS (generally, 1-2 of these sections contained only a handful of scattered HSD2 neurons). In each case the section chosen for analysis contained the prominent rostral cluster of HSD2 neurons, which abuts the fourth ventricle just rostral to the area postrema, as well as a large proportion of the HSD2 neurons flanking and trailing the area postrema caudally. In this section, 6-7 full-thickness confocal stacks (90-120 individual optical planes each) were obtained in order to cover the entire ipsilateral HSD2 neuron population.

In BDA-injected cases, every labeled dendrite emerging from an HSD2-labeled cell body in this tissue section was included for analysis. HSD2-labeled dendrites were followed across image stacks, as necessary, up to their termination within an adjacent image stack from the same tissue section. Individual HSD2-labeled dendrites could be followed over a total length of typically 200-600 μm, well within the range of dendritic lengths measured after filling individual NTS neurons with biocytin in slice preparations (Okada et al., 2006). Dendrites that appeared at the dorsal or ventral cut edge of the tissue and did not emerge from an HSD2 neuron located within this tissue section (i.e. originated from an HSD2 neuron in a tissue section dorsal or ventral to the section chosen for analysis) were not included for analysis. In VGLUT2 +GAD67+HSD2 triple-immunolabeled cases, due to the much larger numbers of labeled contacts quantified per neuron, 10 HSD2 neurons, chosen at random in each case, across the rostrocaudal extent of this group, were analyzed along with all their dendrites for any close contacts (in total 30 neurons from n=3 cases were analyzed for VGLUT2+GAD67+HSD2).

All HSD2 neurons chosen for analysis and all axo-somatic/axo-dendritic close contacts were marked in MetaMorph, and these data were exported to Microsoft Excel for further analysis and presentation. Figures were prepared using Excel and Adobe Illustrator. All data are presented as mean ± SD, except in the case of t-tested group data (rostral versus caudal HSD2 neurons), which are presented as mean ± SEM.

Acknowledgements

Special thanks to Xay Van Nguyen for his expert surgical and histological assistance. Thanks to Sue Aicher for her advice regarding BDA injections into the nodose ganglion, and to Dennis Oakley of the Bakewell Neuroimaging Laboratory at Washington University for advice and assistance with confocal imaging hardware and software.

Grant Support.

1. National Institute of Heart, Lung, and Blood of the NIH, Grant #: HL-25449 (ADL)

2. McDonnell Center for Systems Neuroscience, Washington University School of Medicine, St. Louis, Missouri (JCG)

Literature Cited

Aicher SA, Goldberg A, Sharma S, Pickel VM. mu-opioid receptors are present in vagal afferents and their dendritic targets in the medial nucleus tractus solitarius. J Comp Neurol 2000;422:181–190. [PubMed: 10842226]

Aicher SA, Sharma S, Pickel VM. N-methyl-D-aspartate receptors are present in vagal afferents and their dendritic targets in the nucleus tractus solitarius. Neuroscience 1999;91:119–132. [PubMed: 10336064]

Altschuler SM, Bao XM, Bieger D, Hopkins DA, Miselis RR. Viscerotopic representation of the upper alimentary tract in the rat: sensory ganglia and nuclei of the solitary and spinal trigeminal tracts. J Comp Neurol 1989;283:248–268. [PubMed: 2738198]

Altschuler SM, Escardo J, Lynn RB, Miselis RR. The central organization of the vagus nerve innervating the colon of the rat. Gastroenterology 1993;104:502–509. [PubMed: 8425692]

Altschuler SM, Ferenci DA, Lynn RB, Miselis RR. Representation of the cecum in the lateral dorsal motor nucleus of the vagus nerve and commissural subnucleus of the nucleus tractus solitarii in rat. J Comp Neurol 1991;304:261–274. [PubMed: 1707898]

Andrews WH, Orbach J. Effect of osmotic pressure on spontaneous afferent discharge in the nerves of the perfused rabbit liver. Pflugers Arch 1975;361:89–94. [PubMed: 1239745]

Asada H, Kawamura Y, Maruyama K, Kume H, Ding RG, Kanbara N, Kuzume H, Sanbo M, Yagi T, Obata K. Cleft palate and decreased brain gamma-aminobutyric acid in mice lacking the 67-kDa isoform of glutamic acid decarboxylase. Proc Natl Acad Sci U S A 1997;94:6496–6499. [PubMed: 9177246]

Bailey TW, Hermes SM, Andresen MC, Aicher SA. Cranial visceral afferent pathways through the nucleus of the solitary tract to caudal ventrolateral medulla or paraventricular hypothalamus: target-specific synaptic reliability and convergence patterns. J Neurosci 2006;26:11893–11902. [PubMed: 17108163]

Bailey TW, Hermes SM, Whittier KL, Aicher SA, Andresen MC. A-type potassium channels differentially tune afferent pathways from rat solitary tract nucleus to caudal ventrolateral medulla or paraventricular hypothalamus. J Physiol 2007;582:613–628. [PubMed: 17510187]

Bedi KS, Thomas YM, Davies CA, Dobbing J. Synapse-to-neuron ratios of the frontal and cerebellar cortex of 30-day-old and adult rats undernourished during early postnatal life. J Comp Neurol 1980;193:49–56. [PubMed: 7430433]

Berthoud HR, Kressel M, Neuhuber WL. An anterograde tracing study of the vagal innervation of rat liver, portal vein and biliary system. Anat Embryol (Berl) 1992;186:431–442. [PubMed: 1280009]

Chan RK, Jarvina EV, Sawchenko PE. Effects of selective sinoaortic denervations on phenylephrine-induced activational responses in the nucleus of the solitary tract. Neuroscience 2000;101:165–178. [PubMed: 11068145]

Cooney JR, Hurlburt JL, Selig DK, Harris KM, Fiala JC. Endosomal compartments serve multiple hippocampal dendritic spines from a widespread rather than a local store of recycling membrane. J Neurosci 2002;22:2215–2224. [PubMed: 11896161]

Corbett EK, Sinfield JK, McWilliam PN, Deuchars J, Batten TF. Differential expression of vesicular glutamate transporters by vagal afferent terminals in rat nucleus of the solitary tract: projections from the heart preferentially express vesicular glutamate transporter 1. Neuroscience 2005;135:133–145. [PubMed: 16084661]

Geerling JC, Engeland WC, Kawata M, Loewy AD. Aldosterone target neurons in the nucleus tractus solitarius drive sodium appetite. J Neurosci 2006a;26:411–417. [PubMed: 16407537]

Geerling JC, Kawata M, Loewy AD. Aldosterone-sensitive neurons in the rat central nervous system. J Comp Neurol 2006b;494:515–527. [PubMed: 16320254]

Geerling JC, Loewy AD. Aldosterone-sensitive neurons in the nucleus of the solitary tract: bidirectional connections with the central nucleus of the amygdala. J Comp Neurol 2006a;497:646–657. [PubMed: 16739197]

Geerling JC, Loewy AD. Aldosterone-sensitive neurons in the nucleus of the solitary tract: efferent projections. J Comp Neurol 2006b;497:223–250. [PubMed: 16705681]

Geerling JC, Loewy AD. Aldosterone-sensitive NTS neurons are inhibited by saline ingestion during chronic mineralocorticoid treatment. Brain Res 2006c;1115:54–64. [PubMed: 16935272]

Geerling JC, Loewy AD. Sodium depletion activates the aldosterone-sensitive neurons in the NTS independently of thirst. Am J Physiol Regul Integr Comp Physiol 2007a;292:R1338–1348. [PubMed: 17068161]

Geerling JC, Loewy AD. Sodium deprivation and salt intake activate separate neuronal subpopulations in the nucleus of the solitary tract and the parabrachial complex. J Comp Neurol 2007b;504:379–403. [PubMed: 17663450]

Geerling JC, Sequeira SM, Loewy AD. Increased number of aldosterone-sensitive NTS neurons in Dahl salt-sensitive rats. Brain Res 2005;1065:142–146. [PubMed: 16316636]

Gross PM, Wall KM, Pang JJ, Shaver SW, Wainman DS. Microvascular specializations promoting rapid interstitial solute dispersion in nucleus tractus solitarius. Am J Physiol 1990;259:R1131–1138. [PubMed: 2260724]

Kahrilas PJ, Rogers RC. Rat brainstem neurons responsive to changes in portal blood sodium concentration. Am J Physiol 1984;247:R792–799. [PubMed: 6093603]

Kubin L, Alheid GF, Zuperku EJ, McCrimmon DR. Central pathways of pulmonary and lower airway vagal afferents. J Appl Physiol 2006;101:618–627. [PubMed: 16645192]

Lachamp P, Crest M, Kessler JP. Vesicular glutamate transporters type 1 and 2 expression in axon terminals of the rat nucleus of the solitary tract. Neuroscience 2006;137:73–81. [PubMed: 16216420]

LaMotte CC, Kapadia SE, Shapiro CM. Central projections of the sciatic, saphenous, median, and ulnar nerves of the rat demonstrated by transganglionic transport of choleragenoid-HRP (B-HRP) and wheat germ agglutinin-HRP (WGA-HRP). J Comp Neurol 1991;311:546–562. [PubMed: 1721924]

Loewy, A. Central autonomic pathways. In: Loewy, A.; Spyer, K., editors. Central regulation of autonomic functions. New York: Oxford University Press; 1990. p. 89-103.

Mackay D, Bedi KS. The combined effects of unilateral enucleation and rearing in a “dim” red light on synapse-to-neuron ratios in the rat superior colliculus. J Comp Neurol 1987;256:444–453. [PubMed: 3571516]

Martone ME, Zhang Y, Simpliciano VM, Carragher BO, Ellisman MH. Three-dimensional visualization of the smooth endoplasmic reticulum in Purkinje cell dendrites. J Neurosci 1993;13:4636–4646. [PubMed: 8229189]

Mei N, Condamin M, Boyer A. The composition of the vagus nerve of the cat. Cell Tissue Res 1980;209:423–431. [PubMed: 7407841]

Moechars D, Weston MC, Leo S, Callaerts-Vegh Z, Goris I, Daneels G, Buist A, Cik M, van der Spek P, Kass S, Meert T, D’Hooge R, Rosenmund C, Hampson RM. Vesicular glutamate transporter VGLUT2 expression levels control quantal size and neuropathic pain. J Neurosci 2006;26:12055–12066. [PubMed: 17108179]

Morita H, Yamashita Y, Nishida Y, Tokuda M, Hatase O, Hosomi H. Fos induction in rat brain neurons after stimulation of the hepatoportal Na-sensitive mechanism. Am J Physiol 1997;272:R913–923. [PubMed: 9087655]

Norgren R, Smith GP. Central distribution of subdiaphragmatic vagal branches in the rat. J Comp Neurol 1988;273:207–223. [PubMed: 3417902]

Odermatt A, Arnold P, Stauffer A, Frey BM, Frey FJ. The N-terminal anchor sequences of 11beta-hydroxysteroid dehydrogenases determine their orientation in the endoplasmic reticulum membrane. J Biol Chem 1999;274:28762–28770. [PubMed: 10497248]

Okada T, Yoshioka M, Inoue K, Kawai Y. Local axonal arborization patterns of distinct neuronal types in the caudal nucleus of the tractus solitarius. Brain Res 2006;1083:134–144. [PubMed: 16545781]

Robertson B, Grant G. A comparison between wheat germ agglutinin-and choleragenoid-horseradish peroxidase as anterogradely transported markers in central branches of primary sensory neurones in the rat with some observations in the cat. Neuroscience 1985;14:895–905. [PubMed: 3838806]

Rogers RC, Hermann GE. Central connections of the hepatic branch of the vagus nerve: a horseradish peroxidase histochemical study. J Auton Nerv Syst 1983;7:165–174. [PubMed: 6875186]

Ross CA, Ruggiero DA, Reis DJ. Afferent projections to cardiovascular portions of the nucleus of the tractus solitarius in the rat. Brain Res 1981;223:402–408. [PubMed: 6169408]

Sequeira SM, Geerling JC, Loewy AD. Local inputs to aldosterone-sensitive neurons of the nucleus tractus solitarius. Neuroscience 2006;141:1995–2005. [PubMed: 16828976]

Shekhtman E, Geerling JC, Loewy AD. Aldosterone-sensitive neurons of the nucleus of the solitary tract: multisynaptic pathway to the nucleus accumbens. J Comp Neurol 2007;501:274–289. [PubMed: 17226797]

Smith BN, Dou P, Barber WD, Dudek FE. Vagally evoked synaptic currents in the immature rat nucleus tractus solitarii in an intact in vitro preparation. J Physiol 1998;512(Pt 1):149–162. [PubMed: 9729625]

van der Kooy D, Koda LY, McGinty JF, Gerfen CR, Bloom FE. The organization of projections from the cortex, amygdala, and hypothalamus to the nucleus of the solitary tract in rat. J Comp Neurol 1984;224:1–24. [PubMed: 6715573]

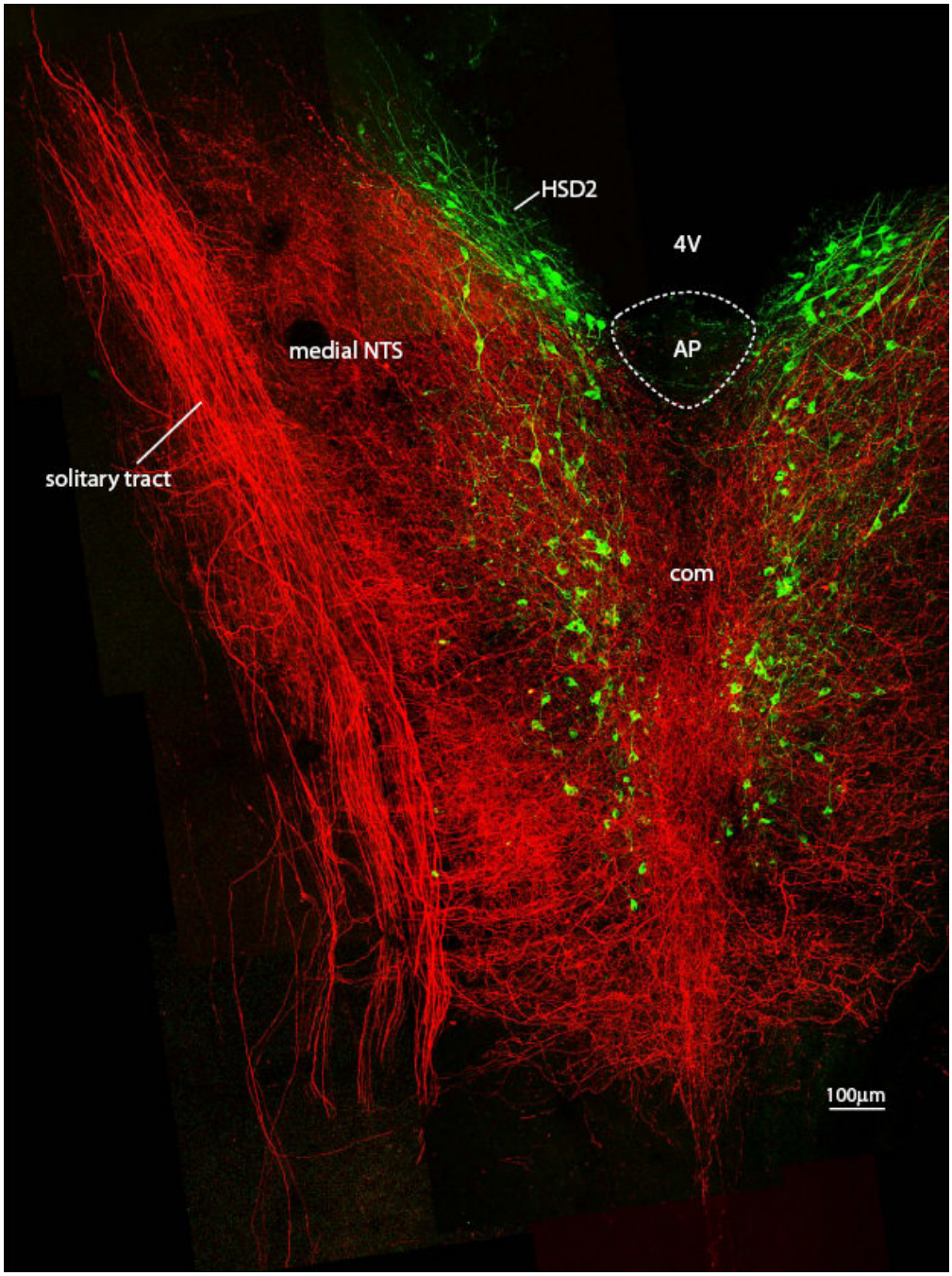

Figure 1.

This horizontal section through the NTS shows the full extent of vagal innervation in this nucleus (BDA-labeled axons, shown in red) relative to the more restricted distribution of HSD2 neurons. Rostrally, clusters of HSD2 neurons border the posterior wall of the fourth ventricle (4V) on either side of the obex, then extend caudally past the area postrema (AP), and continue through the caudal extent of the NTS, where they form two columns flanking the midline commissural subnucleus (com). Note that the rostral clusters of HSD2 neurons lie in a subregion of the NTS with a low density of vagal fibers relative to the caudal extent of this group. Note also that this figure shows the full 200 µm depth of this section as one compressed

plane, and most areas of apparent overlap between vagal fibers and HSD2 neurons did not contain close contacts when examined in individual confocal planes.

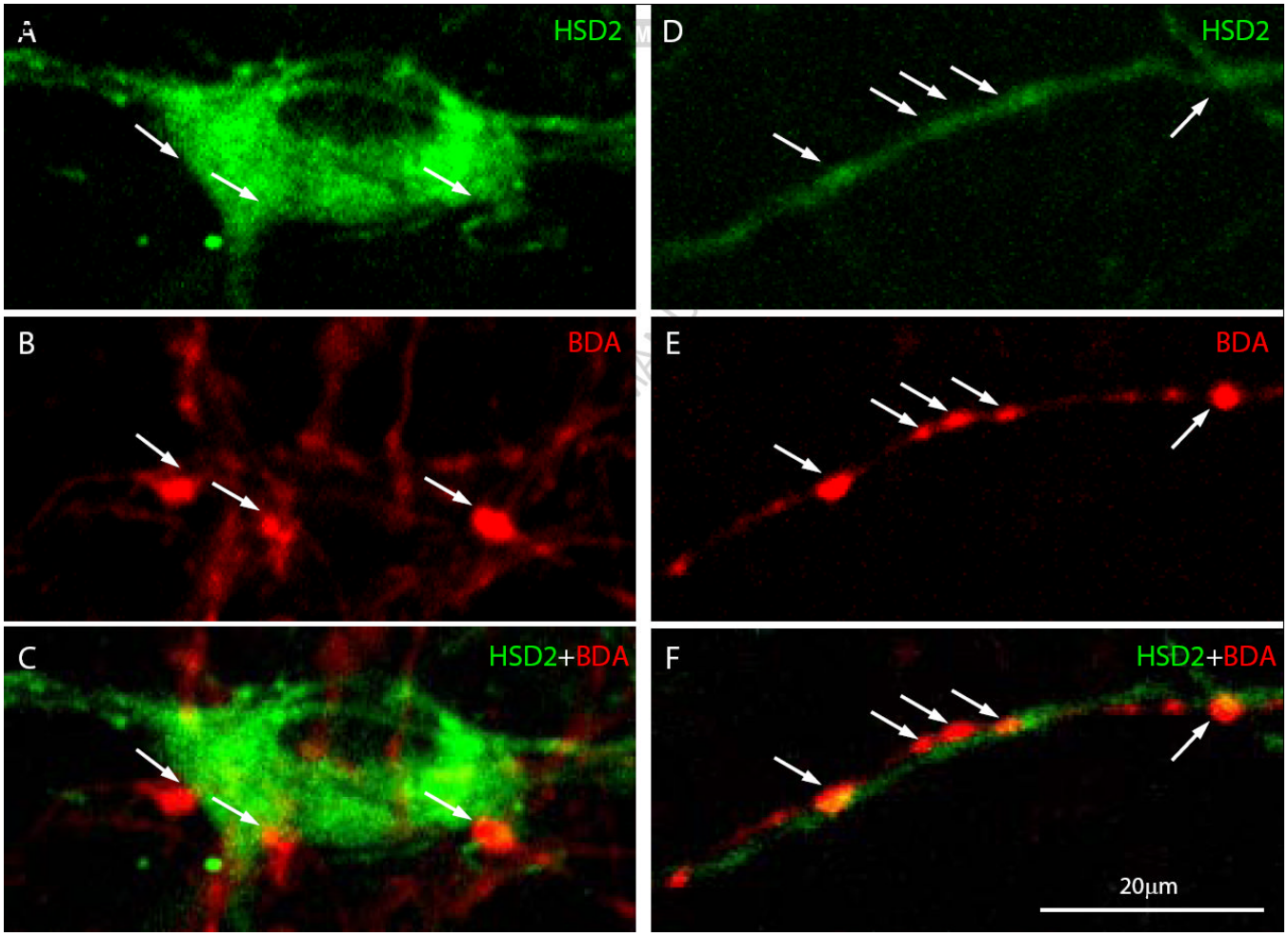

Figure 2.

Examples of axo-somatic (A-C) and axo-dendritic (E-F) close contacts between BDA-labeled boutons (red) and HSD2-labeled neurons (green). Arrows highlight regions of apparent apposition. The partial overlap between some boutons and cells in these images is due to the fact that each represents a 2D projection of 20-25 confocal planes extending ~10 μm in the z-axis, flattened together in order to show greater detail (individual contacts typically do not exhibit any overlapping or co-localized pixels when examined in an individual confocal plane). Note that these select examples represent HSD2 neurons receiving numerous prominent vagal appositions, in contrast to the majority of HSD2 neurons, which received relatively sparse input. 20 μm scale bar in (E) applies to all panels.

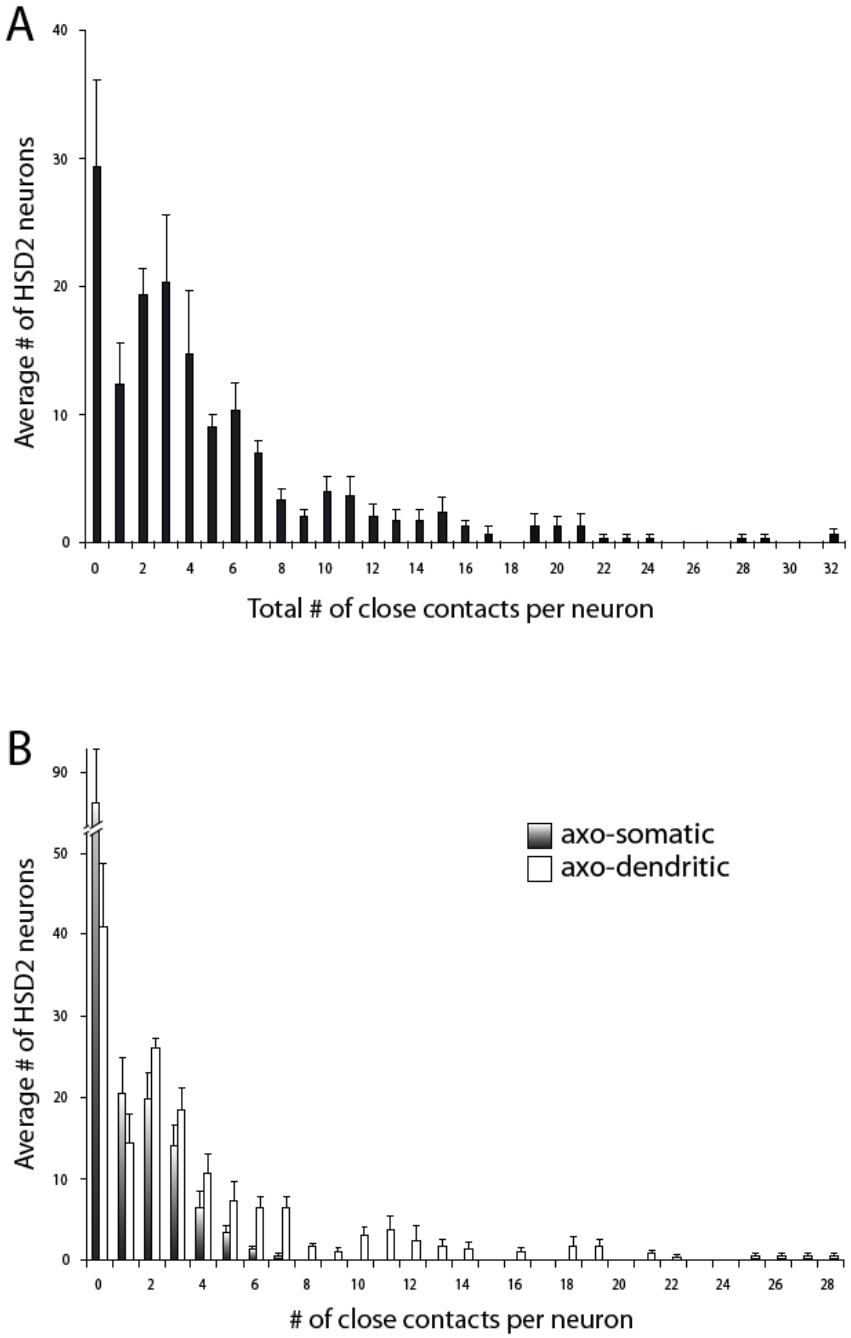

Figure 3.

The histogram in panel (A) shows the frequency distribution of HSD2 neurons receiving different total numbers of contacts from the vagus (averaged across three animals; the average number of HSD2 neurons per case was 151 ± 16.2). Most HSD2 neurons received a small total number of potential synaptic inputs (BDA-labeled close contacts) from the vagus nerve. (B) shows these same frequency data, broken down by type of contact: axo-somatic (gradient fill) or axo-dendritic (white). Note that most HSD2 neurons did not exhibit any axo-somatic contacts and only a few cells received more than a handful, whereas a small number of HSD2 neurons received as many as 28 dendritic contacts. The individual frequency distributions from each case (not shown) were highly similar to this average histogram.

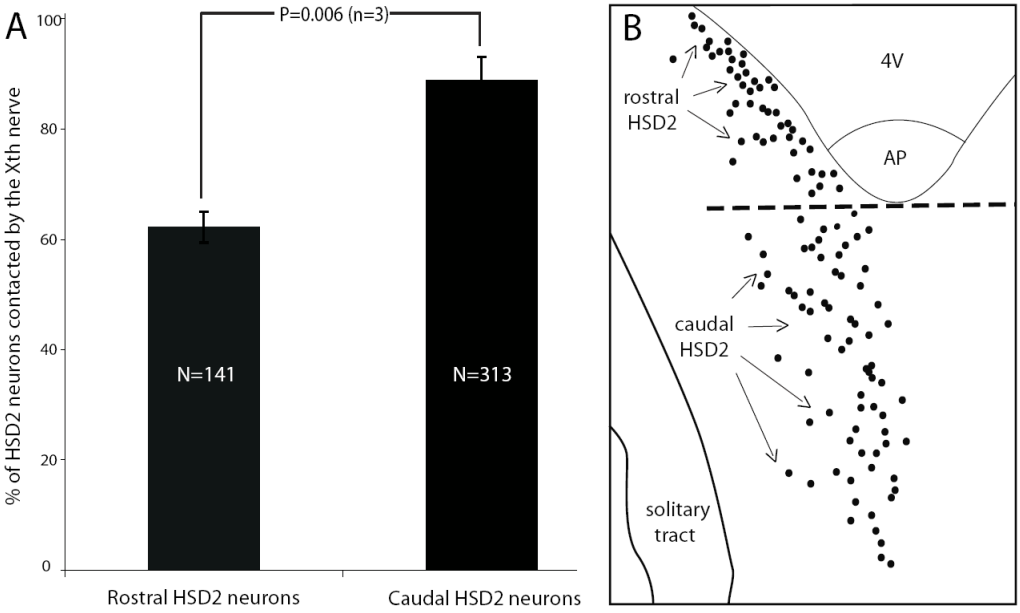

Figure 4.

HSD2 neurons in the rostral and caudal extents of this group exhibit a large difference in the likelihood of input from the vagus nerve. Panel (A) shows a comparison between the percent of HSD2 neurons receiving at least one close contact from a vagal bouton in the rostral versus caudal parts of this population (divided arbitrarily by a mediolateral line through the caudal edge of the area postrema). Across n=3 cases, 87 of 141 rostral HSD2 neurons and 279 of 313 caudal HSD2 neurons received at least one BDA-labeled contact).

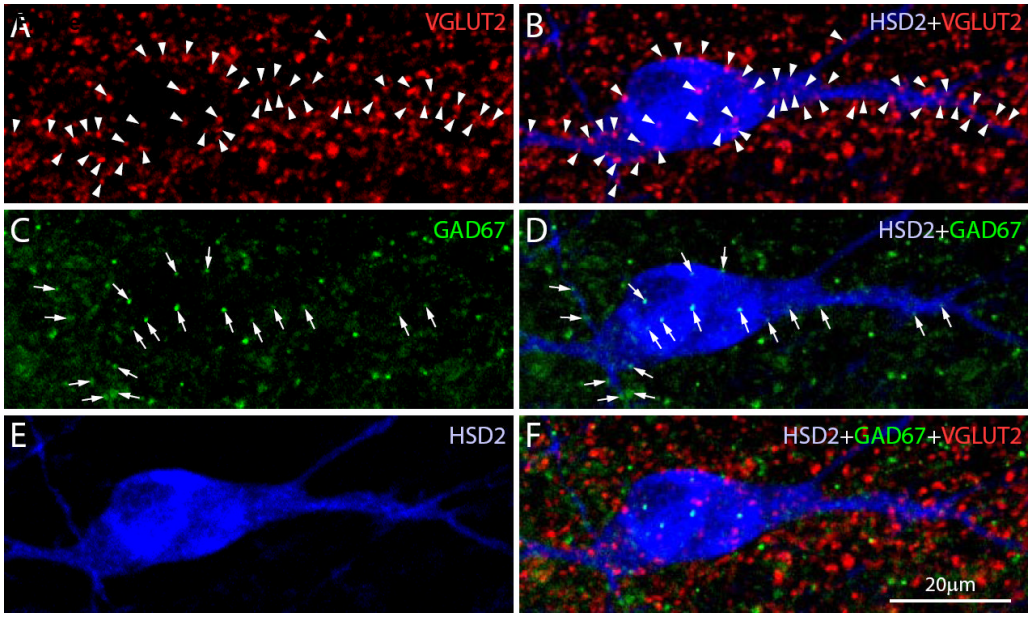

Figure 5.

Many VGLUT2- and GAD67-labeled puncta (representing subtypes of glutamatergic and GABAergic boutons, respectively) contacted every HSD2 neuron. In each case, these contacts greatly exceeding the numbers of vagal contacts found in BDA-injected cases. In this example, a representative HSD2 neuron (blue) receives numerous close contacts from boutons immunolabeled for VGLUT2 (red; arrowheads in A-B) or GAD67 (green; arrows in C-D). These images are two-dimensional maximum-intensity projections extending ~8 um through the z-axis of the tissue section, consisting of 17 confocal planes (each 0.5 μm thick) in order to show the full thickness of this neuron, including boutons that contact its front and back sides. All boutons highlighted in this figure unambiguously contacted the HSD2-ir soma or dendrite as verified in the individual confocal sections that formed these images.

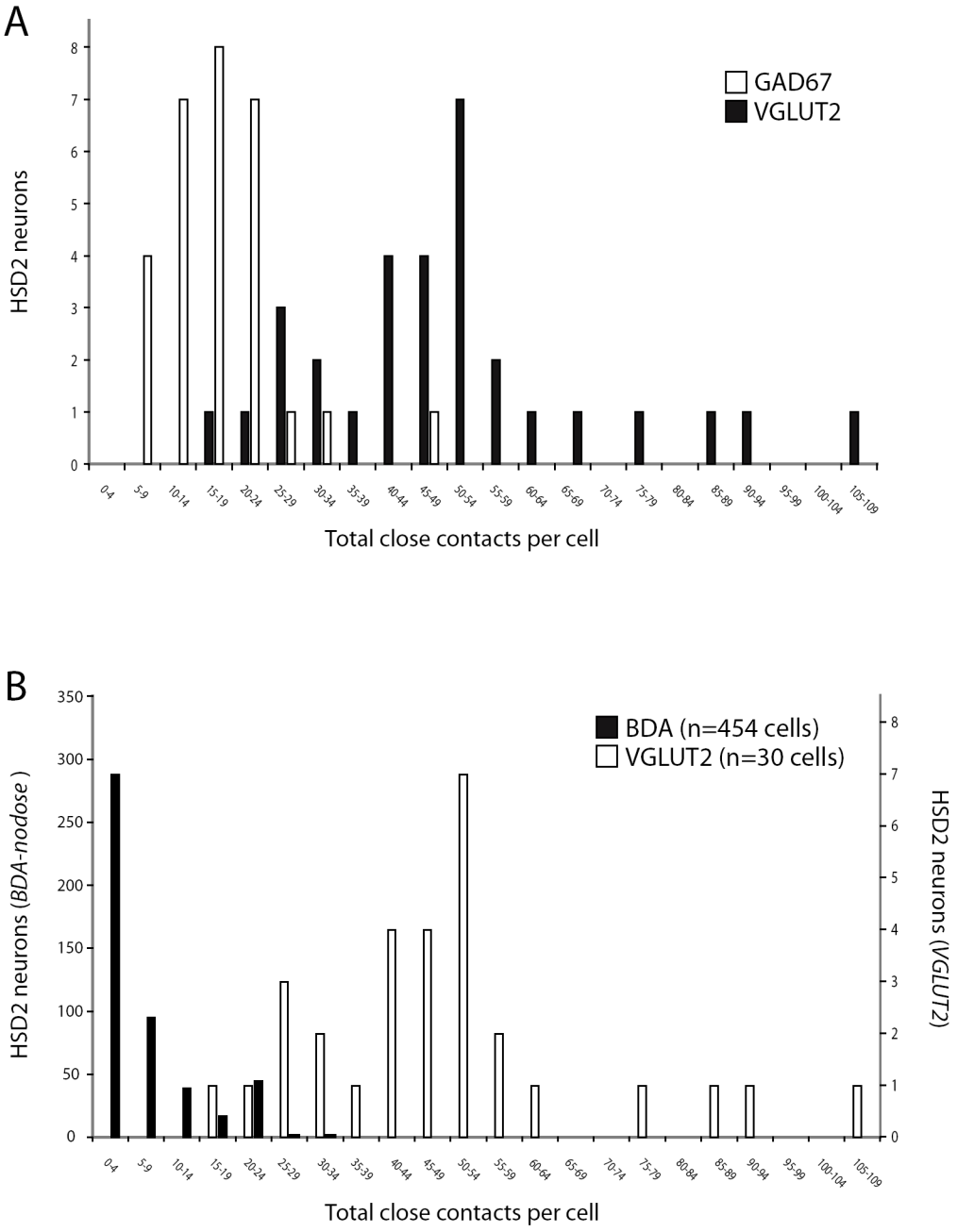

Figure 6.

The overall distributions of HSD2 neurons receiving various numbers of total appositions from VGLUT2- (glutamatergic) or GAD67- (GABAergic) labeled puncta are shown in panel A (2059 total contacts sampled from n=30 HSD2 neurons; 10 each chosen at random from n=3 animals). Panel (B) shows the distribution of HSD2 neurons receiving differing numbers of VLGUT2-labeled contacts in comparison to BDA-labeled (vagal) contacts, re-binned from the dataset shown above. Note that separate axes are used for the numbers of HSD2 neurons receiving BDA versus VGLUT2 contacts (at left and right, respectively) due to the different sample sizes in each analysis (n=454 vs. n=30 total cells sampled).

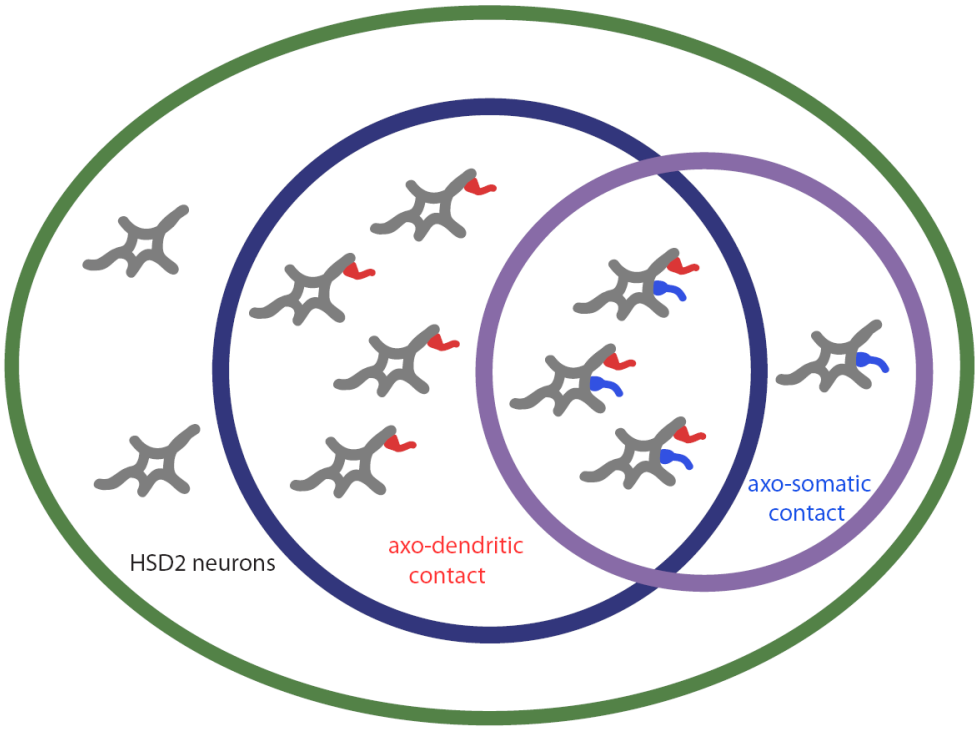

Figure 7.
Venn diagram summarizing HSD2 neurons based on the type(s) of vagal contacts they receive from ipsilateral nodose ganglion cells (NGCs): no apparent contacts (~20%), axo-dendritic contact only (~40%), axo-somatic contact only (~10%), and both types of contact (~30%).